Preventing Weld Hot Cracking by Synchronous Rolling during Welding

The finite element method is used to provide a theoretical model for choosing welding parameters

BY W. LIU, X. TIAN, AND X. ZHANG

ABSTRACT. Based on the mechanical point of view of hot cracking in weldments, a new method, accomplished by synchronous rolling during welding (SRDW) along both sides of the weld at a suitable distance behind the welding arc, has been developed for preventing weld hot cracking. The theory behind this method was also examined. Three-dimensional simulative computations of displacement and strain fields produced by SRDW were carried out by means of the finite element method to reveal the mechanism of the new method and provide a theoretical basis for parameter choice. With a specially developed equipment for welding and synchronous rolling, experiments were performed to investigate the effectiveness and feasibility of this method in preventing weld hot cracking in high-strength aluminum alloy 2024-T4. Results show that weld hot cracking in 2024-Al alloy can be effectively prevented and the mechanical properties of welded joints can also be improved by the new method. It is an important new solution to weld hot cracking in welding of sheet metals.

Introduction

Hot cracking is one of the major problems in welding aluminum alloys, especially high-strength aluminum alloys. Over a long period of time, many research efforts (Refs. 1–10) have been made to solve the problem in welding of materials with high susceptibility to hot cracking. However, in most of them the prevention of weld hot cracking was mainly based on metallurgical means. The possibility and effectiveness of preventing weld hot cracking by mechanical methods have not been fully recognized so far. Some previous studies showed that for hot-cracking susceptible materials the effectiveness of preventing weld hot cracking only by metallurgical methods is limited, in some cases even resulting in degradation of in-service performance. In particular, it is very difficult to prevent liquation cracking in HAZ by metallurgical means because this kind of cracking depends mainly on the characteristics of the base metal.

In this paper, an approach to preventing weld hot cracking was proposed and a new method accomplished by synchronous rolling during welding along both sides of the weld, namely the SRDW method, was developed. The displacements and strains produced by SRDW were computed by means of the finite element method. With the newly developed experimental equipment for welding and synchronous rolling, designated as HNJ-1 machine (Ref. 11), experiments were conducted to investigate the effectiveness and feasibility of preventing weld hot cracking in 2024-Al alloy.

KEY WORDS

Weld Hot Cracking
2024-Al Alloy
Inverse Strain Method
New Approach
Synchronous Rolling
Finite Element Model
Sheet Metal Welding
Welded Joints
Weld Microstructure
Mechanical Properties

Theoretical Analyses

It is well-known that weld hot cracking occurs within the brittleness temperature range (BTR) during weld solidification. The necessary condition for weld hot cracking is that the strain imposed upon the cooling weld or HAZ metal within the BTR is tensile. The sufficient condition for crack occurrence can be stated as the tensile strain rate ($d\varepsilon/dT$) imposed upon the weld or HAZ metal within the BTR is greater than or equal to the critical strain rate for temperature drop (CST), as shown in Fig. 1. The tensile strain can be induced by solidification shrinkage of the weld metal and thermal contraction of the workpiece. In essence, whether cracking will occur or not depends on the competition of two factors. One is the crack-resisting factor, the other is the crack-inducing factor. According to Fig. 1, the hot-cracking resistance of a material during welding may be represented by the width of the BTR and its ductility in the BTR. The narrower the BTR and/or the greater its ductility value in the BTR, the more crack-resistant the weld is. The crack-inducing factor is represented by the tensile strain (ε) imposed upon the weld or HAZ metal within the BTR. In order to prevent hot cracking, one

W. LIU is an Associate Professor in the Department of Materials Science and Engineering, Dalian Railway Institute, Dalian, China. X. TIAN and X. ZHANG are Professors in the School of Materials Science and Engineering, Harbin, China.

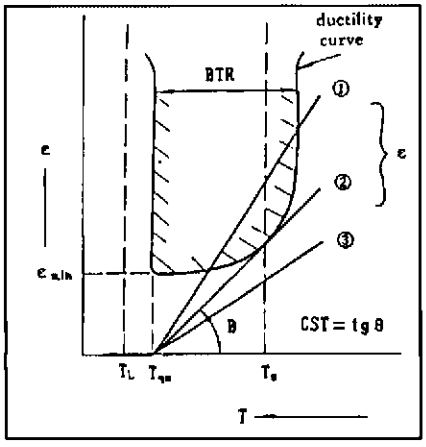

Fig. 1 — Schematic representation of formation condition of weld hot cracking.

can take measures to increase the cracking resistance of the material and/or to depress the crack-inducing factor. Since the crack-resisting factor is relatively constant for a certain combination of base metal and filler metal, it is more suitable to prevent weld hot cracking by taking measures to decrease the crack-inducing factor, *i.e.*, the tensile strain.

As stated above, the presence of tensile strain is recognized as the prerequisite for hot cracking. It is therefore reasonable to expect that cracking will be effectively reduced if an external compressive strain can be exerted on the weld or HAZ metal in the BTR during cooling in order to counteract the crack-inducing tensile strain. The authors designated this new method as the inverse strain method (ISM).

Sufficient condition for hot cracking may be given by:

$$d\varepsilon/dT \geq CST \quad (1)$$

If ε_m is used to denote the tensile strain induced by solidification shrinkage and thermal contraction and ε_c to denote the additional compressive strain produced by ISM, the resultant tensile strain $\varepsilon'm$ actually imposed on the weld or HAZ metal during cooling through the BTR is:

$$\varepsilon'_m = \varepsilon_m + \varepsilon_c \quad (2)$$

Hot cracking will be prevented when the following condition is satisfied:

$$d\,\varepsilon_m/dT + d\,\varepsilon_c/dT < CST \quad (3)$$

while

$$\varepsilon_m + \varepsilon_c = 0 \quad (4)$$

or

$$e_m + e_c < 0 \quad (5)$$

holds, the metal within the BTR will be in a state of no tensile strain or compression, and undoutedly no cracking will occur.

The SRDW method studied in this paper is schematically shown in Fig. 2. Two rollers are set at a suitable distance behind the arc on both sides of the weld. A local rolling force (P) is applied through the two rollers upon both sides of the BTR weld metal. The rolling translational velocity is equal to the welding velocity so that the rolling and welding are synchronous. For simplicity, a unit length of weld is taken for analysis of the transverse strain. Both ends of this unit are restrained as shown in Fig. 3A. The weld metal is subjected to a tensile strain during cooling because of solidification shrinkage and thermal contraction. As the welding temperature distribution is nonuniform and the resistance of metal to straining is lower at higher temperatures, the tensile strain during cooling is concentrated in the weld and HAZ as shown in Fig. 3B. During SRDW the pressure distribution and the distribution of the transverse strain produced by SRDW are qualitatively shown in Fig. 4A and Fig. 4B, respectively. Figure 4 indicates that when the rolling force is exerted upon both sides of the weld, the weld and fusion zone are subjected to a compressive strain (ε_c), which can then counteract the tensile strain (ε_m) that may cause hot cracking. When proper rolling position and rolling force are chosen, enough compressive strain can be produced to reduce or eliminate weld hot cracking.

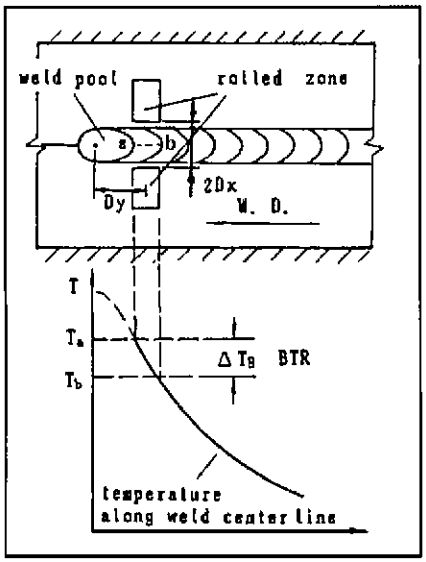

Fig. 2 — Schematic diagram of the SRDW method for preventing weld hot cracking.

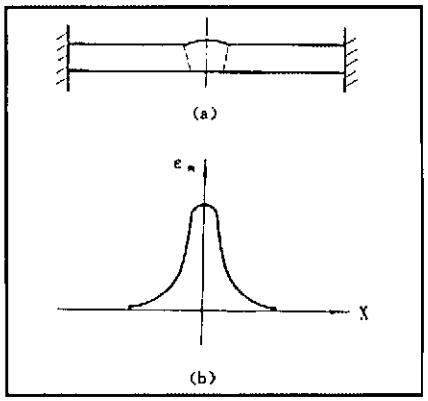

Fig. 3 — Schematic diagram of distribution of transverse welding tensile strain. A — the joint; B — transverse tensile strain.

FEM Computations of Displacement and Strain Fields Produced by SRDW

For the purpose of quantitatively understanding the displacement and strain fields induced by SRDW and then providing a theoretical basis for the proper choice of rolling parameters, 3-D FEM calculations of displacements and strains produced by SRDW were carried out. Simulative experiments were conducted using the Moire fringe technique (Ref. 12) to assess the FEM results.

The Model for Finite Element Analysis

In the SRDW process, metal movement and stresses and strains produced by SRDW vary with time, as the welding temperature does. Therefore, a determination of the complete dynamical response due to SRDW is very complex. Since the rolling velocity is constant, a quasi-stationary state can be reached both for welding and rolling when the plate to be welded is long enough that the effect of ends is negligible. Because only the displacements and strains around the rollers are of interest, a simulative quasi-stationary SRDW problem was analyzed in the present work to reduce the complexity of this analysis. That is to say, static rolling or rather local pressing in a

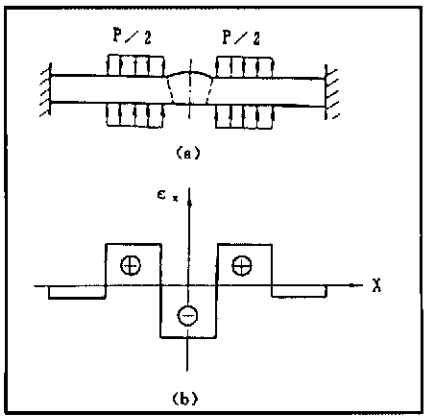

Fig. 4 — Schematic diagram of distribution of transverse strain produced by SRDW. A — the joint; B — transverse strain.

quasi-stationary welding temperature field was considered. The thermomechanical response due to welding was not included in the present study.

The model for this analysis is shown in Fig. 5. Only one half is modeled due to the symmetry. A full three-dimensional analysis is required to completely analyze the problem. The location of rolled zones relative to the welding arc is determined by parameters Dx and Dy. Dx denotes half of the distance between the two rollers, and Dy denotes the distance of the roller axis from the welding arc. The boundary conditions used in the analysis are as follows:

$U_z = 0$, for $z = 0$
(due to the restraint of backing plates)

$U_x = U_y = U_z = 0$, for $x = L_2/2$
(restrained by hydraulic keyboard jigs) (6)

$U_x = 0$, for $x = 0$
(due to the symmetry)

Where, Ux, Uy and Uz are displacement components in the X, Y and Z directions respectively. Prescribed displacements in the rolled zone, whose distribution is shown in Fig. 6, are given as the loads. This treatment is reasonable because the pressure distribution exerted upon the rolled zone is nonuniform and unknown, and is therefore inconvenient to be provided as the external load. As shown in Fig. 6, the dimension S1 is the effective width of the roller, and S2 is determined by the rolling reduction (Wm) and the diameter of the roller.

A finite element mesh used for the numerical calculations is shown in Fig. 7. Eight to ten-node isoparametric hexahedral elements were used for the analysis. Because the rolling-produced in-plane deformation is of particular interest and the plate is thin, one layer of elements was considered in the through-thickness direction (the Z direction). Although strains may be larger in the upper layer of the plate than in the bottom layer when more than one layer of elements are used, the use of one layer of elements in the Z direction represents an average value through the thickness. Gradual mesh refinement was used to concentrate elements in and around the rolled zone. A total of 392 nodes and 170 elements was incorporated in the finite element mesh.

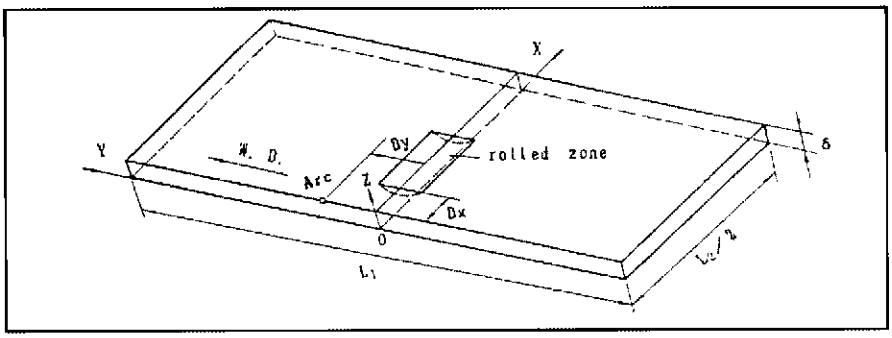

Fig. 5 — Model for finite element analysis.

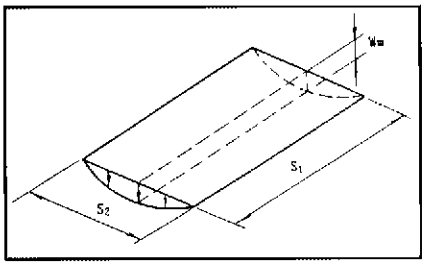

Fig. 6 — Prescribed Z-direction displacements in the rolled zone.

It is very important to consider the influence of the nonuniform welding temperature field on the displacement and strain fields produced by SRDW. For this purpose, the quasi-stationary welding temperature field was first computed. The welding temperature was assumed to be uniform in the plate-thickness direction for the thin plate case. When a coordinate system X'O'Y' moving with the arc is used (X'-axis is perpendicular to, and Y'-axis is along the centerline of the weld bead), under quasi-stationary conditions the heat flow equation becomes:

$$-\rho C_p V \frac{\partial T}{\partial y'} = \frac{\partial}{\partial x'}\left(k\frac{\partial T}{\partial x'}\right) + \frac{\partial}{\partial y'}\left(k\frac{\partial T}{\partial y'}\right) + Q \quad (7)$$

$$Q = \frac{q(x', y')}{\delta} - \frac{2h}{\delta}(T - Ta) \quad (8)$$

where, q(x', y') is the heat flux from the welding arc, which is assumed to take the Gaussian distribution, and is given as

$$q(x', y') = \frac{\eta I U}{2\pi\sigma_q^2} \exp\left(-\frac{x'^2 + y'^2}{2\sigma_q^2}\right) \quad (9)$$

and σ_q = arc heat flux distribution parameter (2.25mm), η = arc efficiency (0.65), I = welding current (120 A), U = arc voltage (18 V), V = welding velocity (4.3 mm/s), δ = plate thickness (2.5 mm), ρ = density of the plate (2.78 g/cm^3), C_p = specific heat, temperature dependent (Ref. 13), k = thermal conductivity, temperature dependent (Ref. 13), h = coefficient of convective and radiative heat loss from the plate surface, temperature dependent (Ref. 13), T_a = ambient temperature.

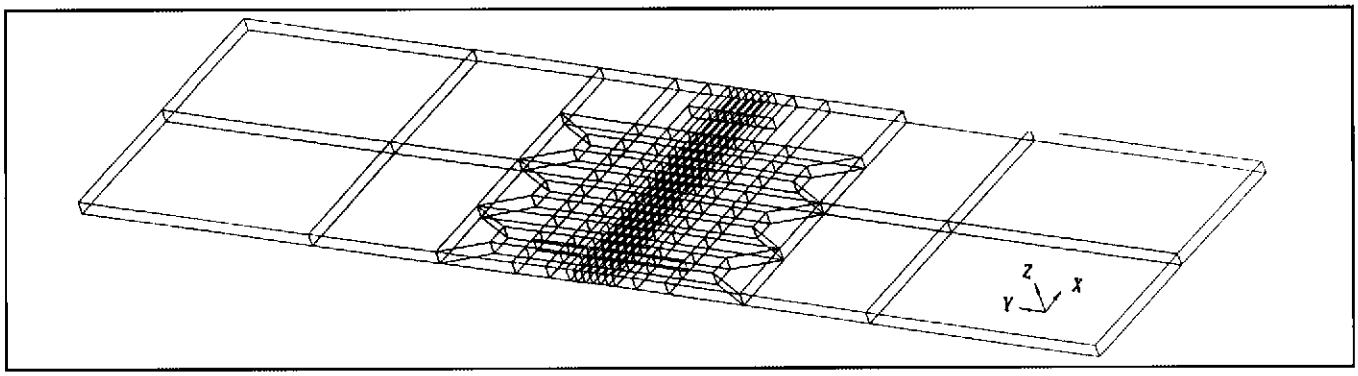

Fig. 7 — The finite element mesh.

Table 1 — Compositions of the Base Metal and Filler Metal Used, wt-%

Materials	Cu	Mg	Mn	Fe	Ti	Si	Zn	B	Al
Base Metal: LY12CZ	4.4	1.5	0.6	<0.3	0.027	0.21	0.09	—	bal.
Filler Metal: Al-Si-Cu	1.8	<0.05	<0.05	<0.3	0.037	4.8	<0.1	0.03	bal.

Table 2 — Material of Element Groups in Dependence of Average Temperature

Group No.	Temperature T, °C	Yield Stress σ_s, MPa	Elastic Modulus E, MPa	Hardening Modulus Ep, MPa	Poisson's Ratio υ
1	<150	284	69000	690	0.31
2	200	240	53500	535	0.31
3	250	186	47500	475	0.31
4	300	113	41500	415	0.31
5	350	64	32000	320	0.31
6	400	34	21000	210	0.31
7	452	10	10000	100	0.31
8	500	1.0	1000	0	0.31
9	550	0.4	400	0	0.31
10	>600	0.1	100	0	0.31

Figure 8 shows the isotherms of the computed quasi-stationary welding temperature field using the finite difference method. With the welding temperature field available, the elements in the model were grouped according to their average temperatures. The temperature dependence of mechanical properties of each group, including the yield strength (σ_s), elastic modulus (E) and hardening modulus (E_p), were accounted for in terms of its average temperature. In this way the influence of the nonuniform welding temperature field was transformed to that of heterogeneity of mechanical properties.

Finite element computations were performed using the multipurpose finite element nonlinear stress analysis computer program ADINA (Ref. 14). Yielding was considered to be governed by the Von Mises' criterion, and plastic flow to be governed by the Prandtl-Reuss law. Isotropic linear strain hardening characteristics of elastoplastic material were assumed. In the solution of nonlinear finite element equations, the BFGS (Broyden-Fletcher-Goldfarb-Shanno) method, a quasi-Newton method, for iteration was used, which proved to be most effective. This method involves updating the coefficient matrix to provide a secant approximation to the matrix from iteration (i-1) to i. The iterative scheme in the BFGS method can he written as (Ref. 15):

$$^{t+\Delta t}K^{(i-1)}\,\underline{\Delta U}^{(i)} = {}^{t+\Delta t}R - {}^{t+\Delta t}F^{(i-1)} \qquad (10)$$

$$^{t+\Delta t}U^{(i)} = {}^{t+\Delta t}U^{(i-1)} + \beta\underline{\Delta U}^{(i)} \qquad (11)$$

Where $^{t+\Delta t}K^{(i-1)}$ = Stiffness matrix employed in iteration (i-1) at time $t^+ \Delta t$; $^{t+\Delta t}R$ = Vector of externally applied nodal point loads at time $t^+ \Delta t$; $^{t+\Delta t}F^{(i-1)}$ = Vector of nodal point forces equivalent to the element stresses in iteration (i-1) at time $t^+ \Delta t$; $^{t+\Delta t}U^{(i)}$, $^{t+\Delta t}U^{(i-1)}$ = Vectors of nodal point displacements in iteration i and (i–1) respectively at time $t+ \Delta t$; $\Delta U^{(i)}$ = Displacement incremental vector defining a "direction" for the actual displacement increment; β = A scalar multiplier employed in the line search in the direction $\underline{\Delta U}^{(i)}$. The updated matrix $^{t+\Delta t}K^{(i)}$ should satisfy the following equation:

$$^{t+\Delta t}K^{(i)}(^{t+\Delta t}U^{(i)} - {}^{t+\Delta t}U^{(i-1)}) = \gamma^{(i)} \qquad (12)$$

Where $\gamma^{(i)}$ is an incremental vector in the out-of-balance loads:

$$\gamma^{(i)} = (^{t+\Delta t}R - {}^{t+\Delta t}F^{(i-1)}) - (^{t+\Delta t}R - {}^{t+\Delta t}F^{(i)}) \qquad (13)$$

and $^{t+\Delta t}K^{(i)}$ can be given in product form:

$$(^{t+\Delta t}K^{-1})^{(i)} = A^{(i)T}(^{t+\Delta t}K^{-1})^{(i-1)}A^{(i)} \qquad (14)$$

where the matrix $A^{(i)}$ is an (n x n) matrix that can be calculated from the known nodal point forces and displacements. In the FEM calculations, the following combined convergence criteria were used:

$$\| \Delta U^{(i)} \|_2 \leq DTOL \cdot \| {}^{t+\Delta t}U^{(i)} \|_2 \qquad (15)$$

$$\Delta U^{(i)T}(^{t+\Delta t}R - {}^{t+\Delta t}F^{(i-1)}) \leq ETOL \cdot \Delta U^{(1)T}(^{t+\Delta t}R - {}^{t}F) \qquad (16)$$

Where, $\Delta U^{(i)} = {}^{t+\Delta t}U^{(i)} - {}^{t+\Delta t}U^{(i-1)}$, DTOL (1 x 10^{-3}) and ETOL (1 x 10^{-5}) are respectively the preset displacement and energy convergence tolerance, and $\|\cdot\|_2$ denotes the Euclidean vector norm.

In the present study, 2024-T4 aluminum alloy sheets were used for the FEM computations and experiments. The chemical composition of the alloy is given in Table 1. The dimensions of the sheet used for this analysis are as follows: length L_1 = 200 mm, width L_2 = 96 mm and thickness δ = 2.5 mm. Elements in the analysis model were divided into 10 groups, with their mechanical properties listed in Table 2. Computations were carried out for different effective widths of the roller and different rolling reductions and relative positions of the rolled zone to the arc.

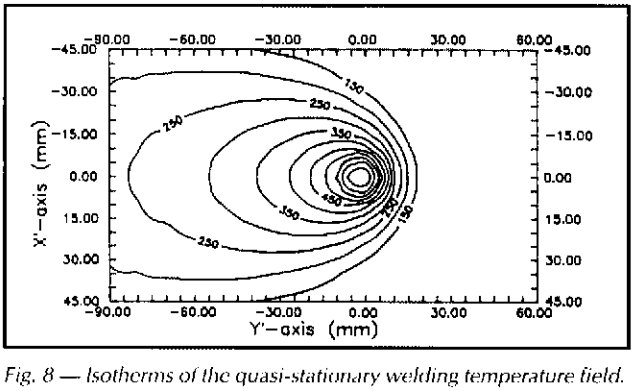

Fig. 8 — Isotherms of the quasi-stationary welding temperature field.

FEM Computational Results and Discussion

Figure 9 shows the undeformed and deformed mesh patterns in the X-Y plane around the rolled zone with a rolling reduction of 0.06 mm and three different Dx values (Dy being 8 mm for all the FEM computations given in the paper). The solid lines represent the undeformed meshes, and the dashed lines represent the deformed meshes, with K_A being the magnification of deformation relative to the actual displacement. An overall deformation pattern in the X-Y plane can be seen from this figure. The in-plane deformation produced by SRDW is not only extremely nonuniform, but is also asymmetrical about the center of the rolled zone due to the nonuniformity of welding temperature distribution. Tensile deformation in the plane is produced in the base metal beneath the roller, and transverse compressive deformation is produced in the weld and bond zone he-

tween the two rollers. As Dx is reduced, the rolled zone becomes closer to the weld metal, and meanwhile the average temperature of the rolled zone increases. Consequently, the compressive deformation produced in the weld metal is much greater with a smaller Dx value. Therefore, the two rollers should be arranged as close as possible.

Transverse displacements (in the X direction) along the transverse section Y=0 and the longitudinal section X=4 mm are plotted in Fig. 10A and 10B, respectively, with Dx being 6 mm and S1 being 18 mm. As shown in Fig. 10A, almost all the transverse plastic flow of metal is directed toward the weld center as a result of the transverse welding temperature gradient. This is determined by the rule of minimum resistance, which says displacement proceeds toward the direction of minimum resistance to deformation. For this reason, a small rolling reduction can make a considerably larger transverse compressive deformation in the weld. Although the plate is laterally restrained in the computational model, it can be inferred from the results in Fig. 10A that little change will take place in the rolling-produced displacement distribution when the restraint is removed. Therefore, the approach should be equally effective in situations where the workpiece is not laterally restrained. It is also shown in Fig. 10 that the absolute values of transverse displacements increase with the increased rolling reduction (Wm), and the maximum transverse displacement at the longitudinal section occurs at Y = 0, *i.e.*, the position corresponding to the roller axis. When the rolling reduction (Wm) is 0.06 mm, the transverse displacement at this position reaches 0.105 mm. As a result of the influence of longitudinal welding temperature distribution, the transverse displacements generated before the roller axis (positive Y-value) are larger than those correspondingly behind the roller axis (minus Y-value).

Figure 11 shows distributions of the transverse strain produced by SRDW along sections Y = 0 and X = 0 (the weld center section), with Dx being 6 mm and S1 being 18 mm. It can be seen that a transverse compressive strain is induced in the weld metal between the two rollers, while this strain component beneath the roller is tensile. Due to the presence of transverse temperature gradient, the maximum absolute magnitude of the compressive strain (2.4%) in the weld is about 3.5 times the tensile strain (0.7%) beneath the roller when the rolling reduction reaches 0.06 mm. From the characteristics of distributions of transverse

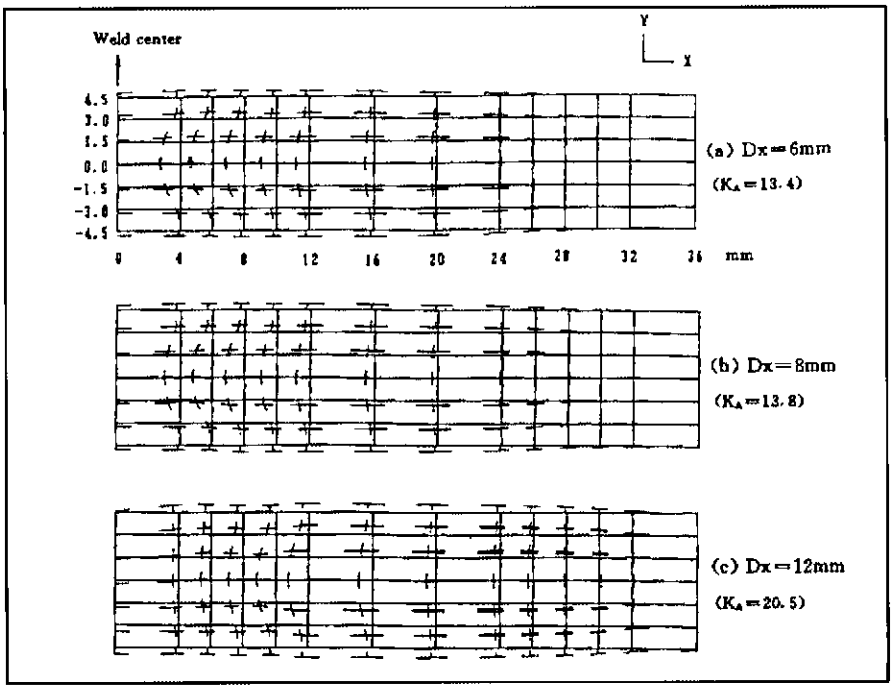

Fig. 9 — Computed deformation in and around the rolled zone in X-Y plane. (Dy = 8 mm, S1 = 18 mm, Wm = 0.06 mm). A — Dx = 6 mm; B — Dx = 8 mm; C— Dx = 12 mm.

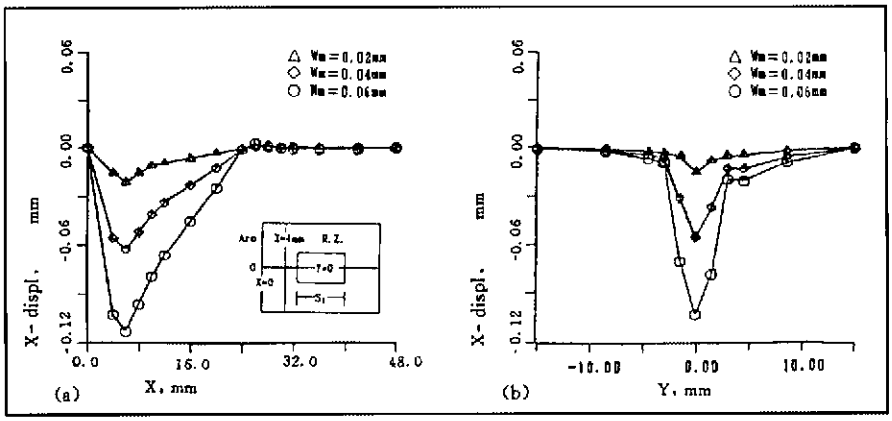

Fig. 10 — Computed transverse displacements produced by SRDW along different sections (Dx = 6 mm, Dy = 8 mm, S1 = 18 mm). A — Along section Y = 0; B — along section X = 4 mm.

compressive strain produced along the weld centerline, it should be noted that a suitable distance (Dy) between the roller axis and the welding arc is important for achieving the best result of prevention of weld hot cracking. Theoretically, the optimum value of Dy should be chosen to keep the distribution of transverse compressive strain produced by SRDW oppositely corresponding to the augmentation of transverse tensile strain behind the weld pool induced by welding, as schematically shown in Fig. 12. According to a computational analysis of weld solidification stress and strain (Ref. 16), the maximum value of transverse tensile strain during solidification in bead-on-plate welds of 2024 aluminum alloy sheets is about 0.8% under generally used welding conditions. Therefore, from the finite element results in Fig. 11, only a rolling reduction of about 0.03 mm is required in order for the rolling-produced compressive strain to completely counteract the crack-inducing tensile strain caused by welding. These FEM computational results demonstrate the effectiveness of the SRDW method.

The computed transverse strain distributions for S1 = 10 mm are shown in Fig. 13, with other parameters being the same. By comparing the results in Fig. 11 anrl Fig. 13, it is indicated that the transverse compression effect of SRDW on the weld metal is not reduced when the effective roller width is decreased from 18 mm to 10 mm. The maximum compressive strain values in the weld are 2.5% for

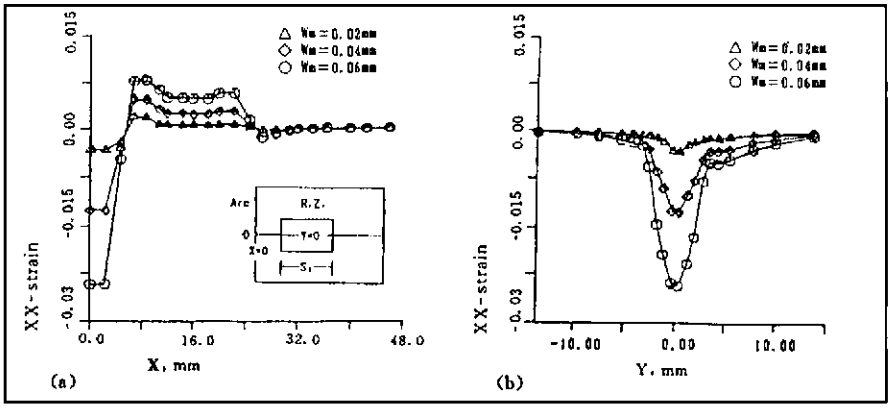

Fig. 11 — Computed distributions of the transverse strain produced by SRDW (Dx = 6 mm, Dy = 8 mm, S1 = 18 mm). A — Along section Y = 0; B — along section X = 0.

S1 = 10 mm and 2.4% for S1 = 18 mm at a rolling reduction of 0.06mm. This is because of the fact that the transverse tensile strain produced in the metal beneath the roller is increased and also more uniformly distributed when the roller width is reduced. Therefore, as far as the effect of induced inverse strain is concerned, a narrower roller should be chosen for use.

Figure 14 shows a comparison of the FEM computed transverse displacements with the experimentally measured transverse displacements along X = 4 mm using the Moire fringe technique. It can be seen that good agreement is obtained between the computational and experimental results.

Experimental Procedure

Experiments were conducted with a special equipment for welding and synchronous rolling (Ref. 11), which was developed for this investigation. LY12CZ (*i.e.*, 2024-T4) aluminum alloy sheet of thickness 2.5 mm was chosen as the base metal. This alloy is well known for its high hot cracking sensitivity and is therefore useful for assessing the effectiveness of the SRDW method. The specimen used for hot cracking tests is shown in Fig. 15. A 15-mm-long slot, at the tip of which welding starts, was made in the specimen to avoid the instability of experimental results (*i.e.*, variability in amount of cracking) which often occurs when welding starts on the edge of a plate. Test specimens were cleaned carefully and then placed into the fixture. Both sides of the specimen parallel to the weld line were clamped tightly by the hydraulic keyboard jig to ensure uniformity of pressure in order to simulate actual production situations where welds are usually made with welding jigs. The keyboard jig had a line of keys on either side acting as holddown fingers. Under hydraulic pressure they operated by friction to restrain the in-plane movement of the metal under them. Full penetration bead-on-plate welds were made in the tests. The GTAW process was used with alternating welding current and argon shielding gas. The welding conditions were 120 A, 18 V, 4.3 mm/s welding speed. Welding and synchronous rolling began 3 s after the arc was struck at the root of the slot. After welding the specimens were examined with dye penetrant inspection and a magnifying glass for any

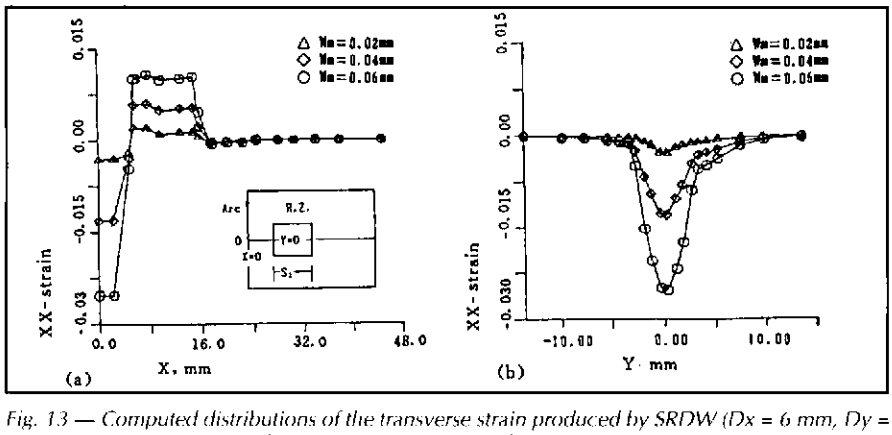

Fig. 13 — Computed distributions of the transverse strain produced by SRDW (Dx = 6 mm, Dy = 8 mm, S1 = 10 mm). A — Along section Y = 0; B — along section X = 0.

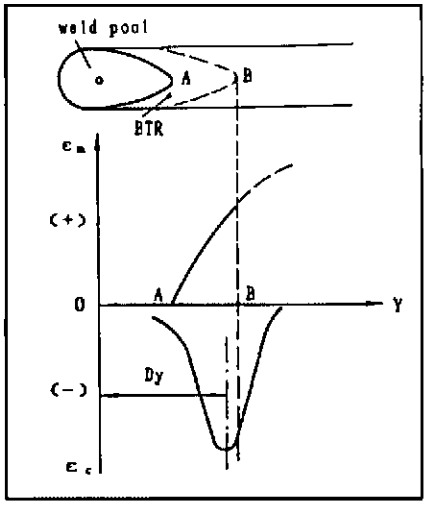

Fig. 12 — Schematic representations of transverse tensile strain induced by welding and the compressive strain produced by SRDW.

cracks. The length of hot cracks was measured with a vernier caliper. The susceptibility to hot cracking was evaluated by the total length (Lcr) of hot cracks. Lcr is given by:

$$Lcr = \sum_{i=1}^{n} Li \tag{17}$$

where n is the number of cracks and Li is the length of crack No. i. Hot cracking tests were conducted with different rolling positions and rolling forces. Tests were repeated three times under identical welding conditions. The average total crack length of the three tests was taken. Tests were also conducted to examine the effects of SRDW on the mechanical properties of welded joints. For this purpose two plates were butt joint welded together with Al-Si-Cu filler metal (Table 1). The dimensions of each plate were 300 mm in length, 150 mm in width and 2.5 mm in thickness. Both tensile tests and cold bend tests were performed after welding. Five samples for each group were tested.

Experimental Results and Discussion

Figure 16 shows the effect of altering the total rolling force on the total hot-crack length. It can be seen that in case of welding without SRDW the susceptibility to hot cracking was very high, the average total crack length was 43 mm with the cracking ratio being as high as 66% (the cracking ratio is defined as the total crack length divided by the weld length). These hot cracks were generally continuous and along the weld centerline. When welds were made with SRDW, the average total crack length de-

creased with increasing rolling force. They exhibited discontinuous, short centerline cracks. No cracking occurred when the rolling force reached 10 kN. In this case, an average rolling reduction of 0.034 mm was produced in the rolled tracks. This value is also comparable to the computed results from the FEM model. Figure 17 shows the results of hot cracking tests by altering the distance (Dy) between the welding arc and the roller axis with a constant rolling force P = 10 kN. It indicates that synchronous rolling position has a remarkable influence on the results of preventing hot cracking by SRDW. As shown in Fig. 17, the best results were achieved (no cracking occurred) when the two rollers were set 6–9 mm behind the welding arc under the welding conditions used in the present study. It was found in the tests that these rolling positions most closely corresponded to the sides of the BTR weld metal immediately behind the weld pool, and a large transverse compressive strain produced by SRDW was consequently imposed upon the BTR metal. It may be worth pointing out that the optimum location of the rollers is dependent on the welding parameters used which influence the temperature field and hence the location of solidifying weld metal zone within BTR.

Figure 18 shows the typical SEM fractographs of weld hot cracks when welding without and with SRDW, and indicates different cracking temperature features. These micrographs were taken in the central part of weld cracks. When welding without SRDW (Fig. 18A), hot cracking occurred in the liquid layers between grains, which implies that in this case cracking occurred at a higher temperature within BTR because of a greater susceptibility to hot cracking — Fig. 1. As shown in Fig. 18B, when welding with SRDW (P = 6 kN) there existed tearing edges and shallow dimples on the hot crack surface. In addition, it was also found in the welding tests that severe cracking occurred in craters of welds made without SRDW, while the crater cracks were eliminated during welding with SRDW.

Figure 19 shows the microstructures in the central region of the transverse section of welds made without and with SRDW. For the weld made without SRDW the examined region was a region which did not exhibit macrocracking. As shown in Fig. 19A, there were micro-cracks in the microstructure made without SRDW, while no cracks were observed in the microstructure made with SRDW — Fig. 19. The microstructures of the HAZ made without and with SRDW are shown in Fig. 20. When welding without SRDW, the grain boundaries in the partially melted zone in Fig. 20A were thickened and there were liquation microcracks, while in case of welding with SRDW these unfavorable phenomena were not found as shown in Fig. 20B. It is clear that the microstructure of the HAZ was also improved by SRDW. The results of tensile and bend tests of welded joints (Table 3) demonstrate that the tensile strength and ductility of welded joints were improved by welding with SRDW because the weld zone was free from microcracks.

Finally, it should be pointed out that the developed process is limited to the butt joint welding of sheet metals and shell structure with regular welds, such as straight welds and circumferential welds of large-diameter thin-walled cylinders.

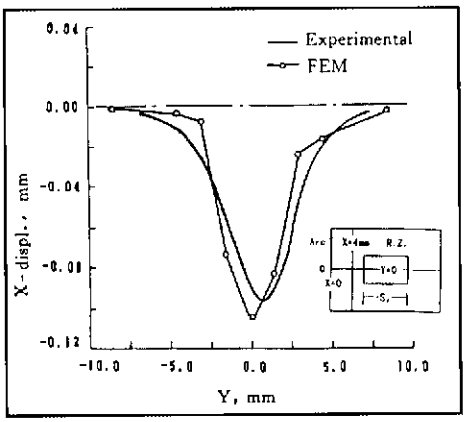

Fig. 14 — Comparison of experimentally measured transverse diplacements with FEM results along section X = 4 mm.

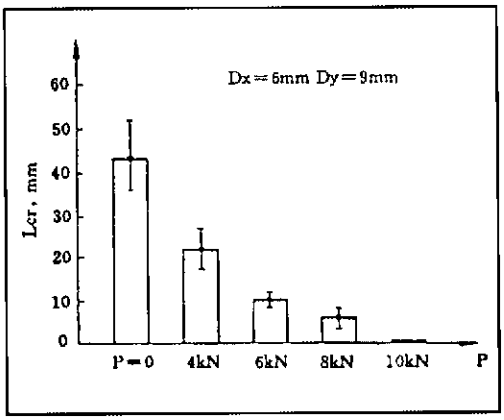

Fig. 15 — Specimen used for hot crack test.

Table 3 — Mechanical Properties of Welded Joints

Rolling Parameters Dx, mm	Dy, mm	P, kN	Tensile Strength σ_b, MPa	Cold Bend Angle α, degree
—	—	0	265.6–299.0 / 284.2	14–18 / 16.5
8	10	4	284.2–323.4 / 306.7	18–23 / 21.0
8	10	6	291.1–336.1 / 308.7	18.5–24 / 21.5
8	10	10	304.8–341 / 323.4	22–24.5 / 23.5

Conclusions

1) Based on the mechanics of hot cracking in weldments, a new method — the SRDW method — has been developed for preventing weld hot cracking. It can be used as a solution to hot cracking in sheet metal welding.

2) A significantly large transverse compressive strain can be produced in the BTR metal by SRDW to counteract the crack-inducing tensile strain and then prevent hot crack formation.

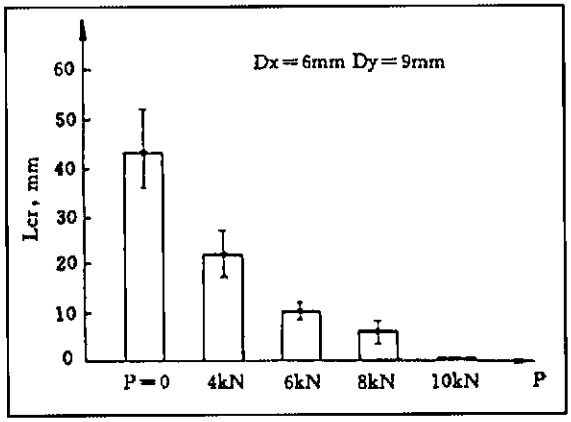

Fig. 16 — Influence of rolling force on hot crack length.

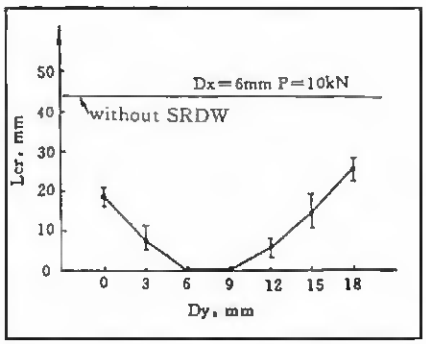

Fig. 17 — Influence of the rolling parameter (Dy) on hot crack length.

3) The welding temperature distribution has a remarkable effect on the displacements and strains produced by SRDW. The transverse temperature gradient intensifies the transverse compression effect of SRDW on the metal within the BTR.

4) Results of both FEM computations and experiments show that weld hot cracking in high strength aluminum alloy LY12CZ (2024-T4) can be effectively prevented by the SRDW method. Mechanical properties of welded joints can also be improved by the method.

5) The parameters of SRDW greatly influence the produced, compressive strain in the BTR metal. It is important to choose appropriate parameters of synchronous rolling for achieving the best results by this method.

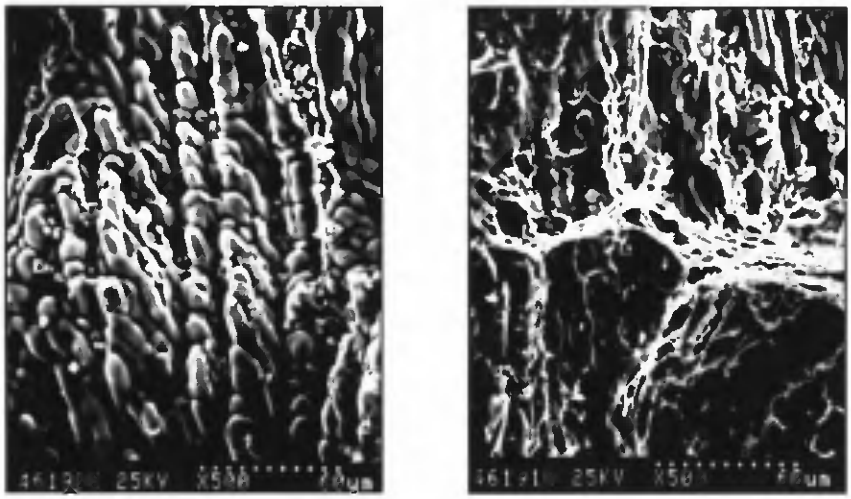

Fig. 18 — SEM fractographs of weld hot cracks in LY12CZ (2024-T4) alloy under different welding conditions. A — without SRDW; B — with SRDW (P = 6 kN).

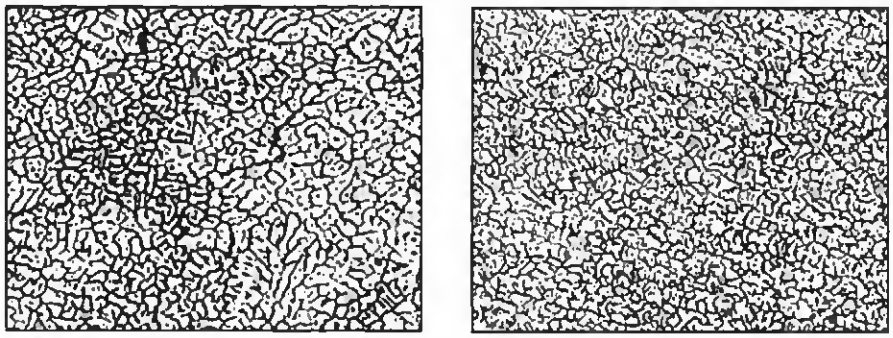

Fig. 19 — Microstructures of bead-on-plate welds of LY12CZ (2024-T4) alloy made when welding without and with SRDW (150X). A — Without SRDW; B — with SRDW (P = 10 kN).

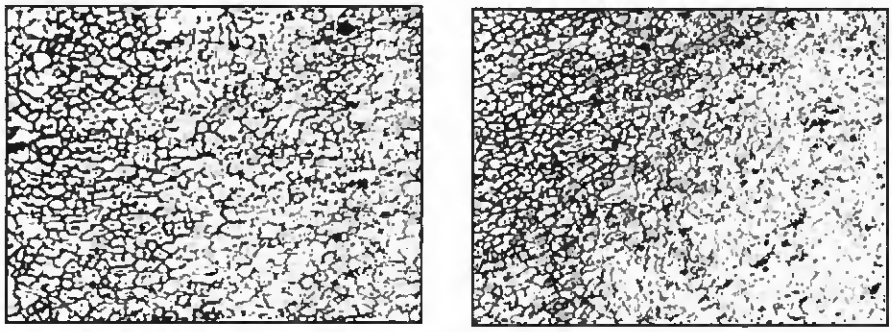

Fig. 20 — Microstructures of HAZ of LY12CZ (2024-T4) alloy welded joints made when welding without and with SRDW (100X). A — without SRDW; B — with SRDW (P = 10kN).

Acknowledgment

The authors are indebted to Prof. Guozhu Zhong, Mr. Zhening Yu and Mr. Yun Peng for their help in carrying out the experiments of this study.

References

1. Dudas, I. H., and Collins, F. R. 1966. Preventing weld cracks in high-strength aluminum alloys. *Welding Journal* 45(6): 241-s to 249-s.

2. Kou, S., and Le, Y. 1985. Alternating grain orientation and weld solidification cracking. *Metallurgical Transactions* 16A(10): 1887–1896.

3. Matsuda, F., Nakata, K., Miyanaga, Y., Kayano, T., and Tsukamoto, K. 1978. Effect of electromagnetic stirring on weld solidification structure of aluminum alloys. *Trans. JWRI* 7(1): 111–127 and 7(2): 182–193.

4. Matsuda, F., Nakata, K., *et al.* 1983. Effect of additional element on weld solidification crack susceptibility of Al-Zn-Mg alloy *Trans. JWRI* 12(1): 81 87.

5. Matsuda, F., Nakata, K., *et al.* 1983. Effect of additional element on weld solidification crack susceptibility of Al-Zn-Mg alloy (Report II). *Trans. JWRI* 12(2): 93102.

6. Matsuda, F., Nakata, K., *et al.* 1984. Effect of additional element on weld solidification crack susceptibility of Al-Zn-Mg alloy (Report III). *Trans. JWRI* 13(1): 5766.

7. Gittos, N. F., and Scott, M. H. 1981. Heat-affected zone cracking Al-Mg-Si alloys. *Welding Journal* 60(6): 95-s to 103-s.

8. Hernandez, I. E., and North, T. H. 1984. The influence of external local heating in preventing cracking during welding of aluminum alloy sheet. *Welding Journal* 63(3): 84-s to 90-s.

9. Zhang, Xiuzhi, *et al.* 1988. Effect of rare-earth element addition on weld hot cracking susceptibility of high-strength aluminum alloy LY12CZ. *Proc. 4th International Conference on Aluminum Weldments.* Tokyo, Japan.

10. Dvornak, M. J., Frost, R. H., and Olson, D. L. 1989. The weldability and grain refinement of Al-2.2Li-2.7Cu. *Welding Journal* 68(8): 327-s to 335-s.

11. Liu, W. 1989. A study of the inverse strain method for preventing weld hot cracking of high-strength aluminum alloy LY12CZ. Ph. D. dissertation. Harbin, Harbin Institute of Technology.

12. Theocaris, P. S. 1969. *Moire Fringes in Strain Analysis.* Permagon press, London.

13. *Handbook for Processing of Light Metallic Materials.* Metallurgical Industry Press, Beijing, China.

14. *ADINA — User's Manuals* 1984. ADINA R&D, Inc.

15. Bathe, K.-J. 1982. *Finite Element Procedures in Engineering Analysis.* Prentice-Hall, Inc., New Jersey.

16. Liu, W. 1995. Computational analysis and prediction of weld solidification cracking. *Computational Materials Science* 4: 211–219.